Supplementary Material (ESI) for Dalton Transaction

SUPPLEMENTARY INFORMATION

Mechanistic investigation of organolanthanide-mediated hydroamination of aminoallenes: A comprehensive computational assessment of various routes for allene activation

Sven Tobisch[a]

[a] *School of Chemistry, University of St Andrews, Purdie Building, North Haugh, St Andrews, KY15 9ST, United Kingdom*

Table S1a Energy profile for 5-*exo* and 6-*endo* ring closure through C=C activation by concomitant proton transfer (*non-insertive mechanism*) in the substrate adduct **3**-S1 of the Cp*$_2$Sm–amido compound [a–d]

ring closure pathway[c]	precursor[d]	TS	product[d]
	0.0/*0.0* (**3**-S1)		
5-*exo* (*anti* pathway)	25.1/*26.6* (**3a'**-S1)	27.1/*30.4*	2-[(*E*)-prop-1-enyl]pyrrolidine –8.8/*–6.5* (**6a**)
5-*exo* (*syn* pathway)	19.4/*20.9* (**3s'**-S1)	27.3/*30.1*	2-[(*Z*)-prop-1-enyl]pyrrolidine –6.5/*–4.0* (**6s**)
6-*endo* (*anti* pathway)	25.1/*26.6* (**3a'**-S1)	32.8/*34.9*	6-ethyltetrahydropyridine –15.1/*–12.2* (**7**)
6-*endo* (*syn* pathway)	19.4/*20.9* (**3s'**-S1)	32.4/*34.3*	6-ethyltetrahydropyridine –15.1/*–12.2* (**7**)

[a] Total barriers and reaction energies are relative to the prevalent form of the Cp*$_2$Sm–amido catalyst complex, *viz*. Cp*$_2$Sm–amido–(substrate)] adduct **3**-S1 and the appropriate number of substrate molecules. [b] Enthalpies and free energies of activation ($\Delta H^{\ddagger}/\Delta G^{\ddagger}$) and reaction ($\Delta H/\Delta G$) are given in kilocalories per mole; numbers in italic type are the Gibbs free energies. [c] See Schemes 3, 4. [d] See the text (or Figs S1–S3) for description of the various isomers of the Cp*$_2$Sm–amido compound and the Cp*$_2$Sm–cycloamine complex, respectively.

Table S1b Energy profile for 5-*exo* and 6- *endo* ring closure through C=C activation by concomitant proton transfer (*non-insertive mechanism*) in the substrate adduct **3**-S2 of the Cp*$_2$Sm–amido compound [a–g]

ring closure pathway[c]	precursor[d]	TS	product[d]
	2.0/*10.1* (**3**-S2)		
5-*exo* (*anti* pathway)	–.–/–.– (**3a'**-S2)[e]	30.8/*41.3*[f]	2-[(*E*)-prop-1-enyl]pyrrolidine
	–.–/–.– (**3a'**-S2)[e]	34.2/*45.1*[g]	–3.4/*4.8* (**6a**-S1)
5-*exo* (*syn* pathway)	–.–/–.– (**3s'**-S1)[e]	30.3/*40.8*[f]	2-[(*Z*)-prop-1-enyl]pyrrolidine
	–.–/–.– (**3s'**-S2)[e]	34.3/*45.3*[g]	0.3/*8.7* (**6s**-S1)
6-*endo* (*anti* pathway)	–.–/–.– (**3a'**-S1)[e]	37.6/*47.6*[f]	6-ethyltetrahydropyridine
	–.–/–.– (**3a'**-S2)[e]	38.3/*48.0*[g]	–4.9/*4.4* (**7**-S1)
6-*endo* (*syn* pathway)	–.–/–.– (**3s'**-S1)[e]	39.5/*49.6*[f]	6-ethyltetrahydropyridine
	–.–/–.– (**3s'**-S2)[e]	39.2/*49.3*[g]	–4.9/*4.4* (**7**-S1)

[a] Total barriers and reaction energies are relative to the prevalent form of the Cp*$_2$Sm–amido catalyst complex, *viz*. Cp*$_2$Sm–amido–(substrate)] adduct **3**-S1 and the appropriate number of substrate molecules. [b] Enthalpies and free energies of activation ($\Delta H^{\ddagger}/\Delta G^{\ddagger}$) and reaction ($\Delta H/\Delta G$) are given in kilocalories per mole; numbers in italic type are the Gibbs free energies. [c] See Schemes 3, 4. [d] See the text (or Figs S1–S3) for description of the various isomers of the Cp*$_2$Sm–amido compound and the Cp*$_2$Sm–azacycle intermediates, respectively. [e] All attempts to locate this species were unsuccessful. [f] The central trajectory (see Scheme S1). [g] The frontal trajectory (see Scheme S1).

Table S2a Energy profile for 5-*exo* and 6-*endo* ring closure through C=C insertion into the Sm–N σ-bond (*insertive mechanism*) in the substrate-free form of the Cp^*_2Sm–amido compound [a–d]

ring closure pathway[c]	precursor[d]	TS	product[d]
	13.9/*6.6* (**3**)		
5-*exo* (*anti* pathway)	18.0/*13.2* (**3a'**)	21.2/17.5	6.9/*2.3* (**4a**)
5-*exo* (*syn* pathway)	14.0/*9.3* (**3s'**)	19.4/*15.7*	7.6/*3.0* (**4s**)
6-*endo* (*anti* pathway)	18.0/*13.2* (**3a'**)	27.7/*23.7*	0.2/–3.5 (**5a**) 6.1/2.4(**5a'**)
6-*endo* (*syn* pathway)	14.0/*9.3* (**3s'**)	28.9/*24.9*	6.0/1.9 (**5s**) –0.5/–4.6 (**5s'**)

[a] Total barriers and reaction energies are relative to the prevalent form of the Cp^*_2Sm–amido catalyst complex, *viz*. Cp^*_2Sm–amido–(substrate)] adduct **3**-S1 and the appropriate number of substrate molecules. [b] Enthalpies and free energies of activation ($\Delta H^{\ddagger}/\Delta G^{\ddagger}$) and reaction ($\Delta H/\Delta G$) are given in kilocalories per mole; numbers in italic type are the Gibbs free energies. [c] See Schemes 4, 5. [d] See the text (or Figs S4, S5) for description of the various isomers of the Cp^*_2Sm–amido compound and the Cp^*_2Sm–azacycle intermediate, respectively.

Table S2b Energy profile for 5-*exo* and 6-*endo* ring closure through C=C insertion into the Sm–N σ-bond (*insertive mechanism*) in the substrate adduct **3**-S1 of the Cp^*_2Sm–amido compound [a–f]

ring closure pathway[c]	precursor[d]	TS	product[d]
	0.0/*0.0* (**3**-S1)		
5-*exo* (*anti* pathway)	25.1/*26.6* (**3a'**-S1)[e]	28.0/*31.0*[e]	6.5/*9.5* (**4a**-S1)[e]
	24.0/*26.0* (**3a'**-S1)[f]	26.6/*29.7*[f]	5.1/*8.3* (**4a**-S1)[f]
5-*exo* (*syn* pathway)	19.4/*20.9* (**3s'**-S1)[e]	23.7/*26.7*[e]	3.8/*6.9* (**4s**-S1)[e]
	17.9/*20.4* (**3s'**-S1)[f]	23.0/*26.0*[f]	4.0/*7.2* (**4s**-S1)[f]
6-*endo* (*anti* pathway)	25.1/*26.6* (**3a'**-S1)[e]	31.0/*33.5*[e]	–3.6/*–0.1* (**5a**-S1)[e] –2.7/*0.4* (**5a'**-S1)[e]
	24.0/*26.0* (**3a'**-S1)[f]	30.6/*33.0*[f]	0.5/*3.0* (**5a**-S1)[f] 1.3/*5.3* (**5a'**-S1)[f]
6-*endo* (*syn* pathway)	19.4/*20.9* (**3s'**-S1)[e]	28.9/*31.4*[e]	0.7/*4.2* (**5s**-S1)[e] 3.9/*6.9* (**5s'**-S1)[e]
	17.9/*20.4* (**3s'**-S1)[f]	32.0/*34.4*[f]	–3.7/*–1.1* (**5s**-S1)[f] – 3.1/*0.9* (**5s'**-S1)[f]

[a] Total barriers and reaction energies are relative to the prevalent form of the Cp^*_2Sm–amido catalyst complex, *viz*. Cp^*_2Sm–amido–(substrate)] adduct **3**-S1 and the appropriate number of substrate molecules. [b] Enthalpies and free energies of activation ($\Delta H^{\ddagger}/\Delta G^{\ddagger}$) and reaction ($\Delta H/\Delta G$) are given in kilocalories per mole; numbers in italic type are the Gibbs free energies. [c] See Schemes 4, 5. [d] See the text (or Figs S4, S5) for description of the various isomers of the Cp^*_2Sm–amido compound and the Cp^*_2Sm–azacycle intermediate, respectively. [e] The frontal trajectory (see Scheme S2). [f] The lateral trajectory (see Scheme S2).

Table S2c Energy profile for 5-*exo* and 6- *endo* ring closure through C=C insertion into the Sm–N σ-bond (*insertive mechanism*) in the substrate adduct **3**-S2 of the Cp*$_2$Sm–amido compound [a–h]

ring closure pathway[c]	precursor[d]	TS	product[d]
	2.0/*10.1* (**3**-S2)		
5-*exo* (*anti* pathway)	–.–/–.– (**3a'**-S2)[e]	46.9/*56.6*[f]	20.1/*30.2* (**4a**-S2)[f]
	–.–/–.– (**3a'**-S2)[e]	53.5/*62.7*[g]	25.7/*36.0* (**4a**-S2)[g]
	–.–/–.– (**3a'**-S2)[e]	52.3/*61.8*[h]	29.8/*40.1* (**4a**-S2)[h]
5-*exo* (*syn* pathway)	–.–/–.– (**3s'**-S2)[e]	42.2/*51.9*[f]	16.5/*26.6* (**4s**-S2)[f]
	–.–/–.– (**3s'**-S2)[e]	48.1/*57.3*[g]	19.9/*30.2* (**4s**-S2)[g]
	–.–/–.– (**3s'**-S2)[e]	47.3/*56.8*[h]	27.6/*37.8* (**4a**-S2)[h]
6-*endo* (*anti* pathway)	–.–/–.– (**3a'**-S2)[e]	48.6/*58.3*[f]	9.5/*19.5* (**5a**-S2)[f]
			1.8/*12.0* (**5a'**-S2)[f]
	–.–/–.– (**3a'**-S2)[e]	55.8/*65.3*[g]	
	–.–/–.– (**3a'**-S2)[e]	53.8/*63.7*[g]	
6-*endo* (*syn* pathway)	–.–/–.– (**3s'**-S2)[e]	47.5/*57.2*[f]	15.1/*25.9* (**5s**-S2)[f]
			9.2/*19.7* (**5s'**-S2)[f]
	–.–/–.– (**3s'**-S2)[e]	56.3/*65.8*[g]	
	–.–/–.– (**3s'**-S2)[e]	54.8/*64.7*[h]	

[a] Total barriers and reaction energies are relative to the prevalent form of the Cp*$_2$Sm–amido catalyst complex, *viz*. Cp*$_2$Sm–amido–(substrate)] adduct **3**-S1 and the appropriate number of substrate molecules. [b] Enthalpies and free energies of activation ($\Delta H^{\ddagger}/\Delta G^{\ddagger}$) and reaction ($\Delta H/\Delta G$) are given in kilocalories per mole; numbers in italic type are the Gibbs free energies. [c] See Schemes 4, 5. [d] See the text (or Figs S4, S5) for description of the various isomers of the Cp*$_2$Sm–amido compound and the Cp*$_2$Sm–azacycle intermediate, respectively. [e] All attempts to locate this species were unsuccessful. [f] The central trajectory (see Scheme S2). [g] The frontal trajectory (see Scheme S2). [h] The lateral trajectory (see Scheme S2).

Table S3a Energy profile for isomerisation of the *exo*-methylene tether in the substrate-free five-membered Cp*$_2$Sm–azacycle intermediate **4** [a–c]

ring closure pathway[c]	*anti* methylene	TS	*syn* methylene
5-*exo*	6.9/*2.3* (**4a**)	54.8/*50.2*	7.6/*3.0* (**4s**)

[a] Total barriers and reaction energies are relative to the prevalent form of the Cp*$_2$Sm–amido catalyst complex, *viz*. Cp*$_2$Sm–amido–(substrate)] adduct **3**-S1 and the appropriate number of substrate molecules. [b] Enthalpies and free energies of activation ($\Delta H^{\ddagger}/\Delta G^{\ddagger}$) and reaction ($\Delta H/\Delta G$) are given in kilocalories per mole; numbers in italic type are the Gibbs free energies. [c] See Schemes 4, 5.

Table S3b Energy profile for isomerisation of the *exo*-methylene tether in the substrate adduct **4**-S1 of the five-membered Cp*$_2$Sm–azacycle intermediate [a–e]

ring closure pathway[c]	*anti* methylene	TS	*syn* methylene
5-*exo*	6.5/*9.5* (**4a**-S1)[d]	52.7/*56.0*	3.8/*6.9* (**4s**-S1)
	5.1/*8.3* (**4a**-S1)[e]	58.5/*61.8*	4.0/*7.2* (**4s**-S1)

[a] Total barriers and reaction energies are relative to the prevalent form of the Cp*$_2$Sm–amido catalyst complex, *viz*. Cp*$_2$Sm–amido–(substrate)] adduct **3**-S1 and the appropriate number of substrate molecules. [b] Enthalpies and free energies of activation ($\Delta H^{\ddagger}/\Delta G^{\ddagger}$) and reaction ($\Delta H/\Delta G$) are given in kilocalories per mole; numbers in italic type are the Gibbs free energies. [c] See Schemes 4, 5. [d] To engage the isomer of **4**-S1 generated through the frontal ring-closure trajectory (see Scheme S2). [e] To engage the isomer of **4**-S1 generated through the lateral ring-closure trajectory (see Scheme S2).

Table S3c Energy profile for isomerisation of the *exo*-methylene tether in the substrate-adduct **4**-S2 of the five-membered Cp*$_2$Sm–azacycle intermediate [a–f]

ring closure pathway[c]	*anti* methylene	TS	*syn* methylene
5-*exo*	20.1/*30.2* (**4a**-S2)[d]	69.5/*79.1*	16.5/*26.6* (**4s**-S2)
	25.7/*36.0* (**4a**-S2)[e]		19.9/*30.2* (**4s**-S2)
	29.8/*40.1* (**4a**-S2)[f]		27.6/*37.8* (**4s**-S2)

[a] Total barriers and reaction energies are relative to the prevalent form of the Cp*$_2$Sm–amido catalyst complex, *viz*. Cp*$_2$Sm–amido–(substrate)] adduct **3**-S1 and the appropriate number of substrate molecules. [b] Enthalpies and free energies of activation ($\Delta H^{\ddagger}/\Delta G^{\ddagger}$) and reaction ($\Delta H/\Delta G$) are given in kilocalories per mole; numbers in italic type are the Gibbs free energies. [c] See Schemes 4, 5. [d] To engage the isomer of **4**-S2 generated through the central ring-closure trajectory (see Scheme S2). [e] To engage the isomer of **4**-S2 generated through the frontal ring-closure trajectory (see Scheme S2). [f] To engage the isomer of **4**-S2 generated through the lateral ring-closure trajectory (see Scheme S2).

Table S4a Energy profile for aminolysis in the substrate adduct **4**-S1 of the Cp*$_2$Sm–azacycle intermediate to afford Cp*$_2$Sm–amido–cycloamine compound **6** [a–f]

aminolysis pathway[c]	**4**-S1[d]	TS	product[d]
H-trf onto C^6 of **4a** **4a**-S1 → **6a**	6.5/*9.5*[e]	15.6/*19.2*[e,f]	2-[(*E*)-prop-1-enyl]pyrrolidine –8.8/*–6.5* (**6a**)
H-trf onto C^6 of **4s** **4s**-S1 → **6s**	3.8/*6.9*[e]	15.0/*18.8*[e,f]	2-[(*Z*)-prop-1-enyl]pyrrolidine –6.5/*–4.0* (**6s**)

[a] Total barriers and reaction energies are relative to the prevalent form of the Cp*$_2$Sm–amido catalyst complex, *viz*. Cp*$_2$Sm–amido–(substrate)] adduct **3**-S1 and the appropriate number of substrate molecules. [b] Enthalpies and free energies of activation ($\Delta H^{\ddagger}/\Delta G^{\ddagger}$) and reaction ($\Delta H/\Delta G$) are given in kilocalories per mole; numbers in italic type are the Gibbs free energies. [c] See Schemes 4, 5. [d] See the text (or Fig. S6) for description of the various isomers of the amine adduct **4**-S1 and of the Cp*$_2$Sm–amido–cycloamine product species, respectively. [e] To engage the isomer of **4**-S1 generated through the frontal ring-closure trajectory (see Scheme S2). [f] The isomer of **4**-S1 generated through the lateral ring-closure trajectory cannot traverse this pathway.

Table S4b Energy profile for aminolysis in the substrate adduct **4**-S2 of the Cp*$_2$Sm–azacycle intermediate to afford Cp*$_2$Sm–amido–cycloamine substrate-adduct **6**-S1 [a–c]

aminolysis pathway[c]	**4**-S2[d]	TS	product[d]
H-trf onto C^6 of **4a** **4a**-S2 → **6a**-S1	20.1/*30.2*[e] 25.7/*36.0*[f]	28.4/*38.4*[e,g] 28.4/*39.2*[f,g]	2-[(*E*)-prop-1-enyl]pyrrolidine –3.4/*4.8* (**6a**-S1)
H-trf onto C^8 of **4s** **4s**-S2 → **6s**-S1	16.5/*26.6*[e] 19.9/*30.2*[f]	28.2/*37.7*[e,g] 27.4/*38.0*[f,g]	2-[(*Z*)-prop-1-enyl]pyrrolidine 0.3/*8.7* (**6s**-S1)

[a] Total barriers and reaction energies are relative to the prevalent form of the Cp*$_2$Sm–amido catalyst complex, *viz*. Cp*$_2$Sm–amido–(substrate)] adduct **3**-S1 and the appropriate number of substrate molecules. [b] Enthalpies and free energies of activation ($\Delta H^{\ddagger}/\Delta G^{\ddagger}$) and reaction ($\Delta H/\Delta G$) are given in kilocalories per mole; numbers in italic type are the Gibbs free energies. [c] See Schemes 4, 5. [d] See the text (or Fig. S6) for description of the various isomers of the amine adduct **4**-S2 and of the Cp*$_2$Sm–amido–cycloamine product species, respectively. [e] To engage the isomer of **4**-S2 generated through the central ring-closure trajectory (see Scheme S2). [f] To engage the isomer of **4**-S2 generated through the frontal ring-closure trajectory (see Scheme S2). [g] The isomer of **4**-S2 generated through the lateral ring-closure trajectory cannot traverse this pathway.

Table S5a Energy profile for aminolysis in the substrate adduct **5'**-S1 of the Cp*$_2$Sm–azacycle intermediate to afford Cp*$_2$Sm–amido–cycloamine compound **8** [a–f]

aminolysis pathway[c]	**5'**-S1[d]	TS	product[d]
H-trf onto C^5 of **5a'** **5a'**-S1 → **8a**	1.3/*5.3*[e]	10.8/*15.1*[e,f]	2*E*-ethylidenepiperidine –13.8/*–10.8* (**8a**)
H-trf onto C^5 of **5s'** **5s'**-S1 → **8s**	–3.1/*0.9*[e]	4.5/*8.7*[e,f]	2*Z*-ethylidenepiperidine –13.0/*–10.0* (**8s**)

[a] Total barriers and reaction energies are relative to the prevalent form of the Cp*$_2$Sm–amido catalyst complex, *viz*. Cp*$_2$Sm–amido–(substrate)] adduct **3**-S1 and the appropriate number of substrate molecules. [b] Enthalpies and free energies of activation ($\Delta H^{\ddagger}/\Delta G^{\ddagger}$) and reaction ($\Delta H/\Delta G$) are given in kilocalories per mole; numbers in italic type are the Gibbs free energies. [c] See Schemes 4, 5. [d] See the text (or Fig. S7) for description of the various isomers of the amine adduct **5'**-S1 and of the Cp*$_2$Sm–amido–cycloamine product species, respectively. [e] To engage the isomer of **5'**-S1 generated through the lateral ring-closure trajectory (see Scheme S2). [f] The isomer of **5'**-S1 generated through the frontal ring-closure trajectory cannot traverse this pathway.

Table S5b Energy profile for aminolysis in the substrate adduct **5'**-S2 of the Cp*$_2$Sm–azacycle intermediate to afford Cp*$_2$Sm–amido–cycloamine substrate-adduct **8**-S1 [a–c]

aminolysis pathway[c]	**5'**-S2[d]	TS	product[d]
H-trf onto C^5 of **5a'** **5a'**-S2 → **8a**-S1	1.8/*12.0*[e]	10.4/*21.0*[e,g] 11.2/*21.7*[f,g]	2*E*-ethylidenepiperidine –5.9/*2.8* (**8a**-S1)
H-trf onto C^5 of **5s'** **5s'**-S2 → **8s**-S1	9.2/*19.7*[e]	11.2/*22.1*[e,g] 12.2/*23.1*[f,g]	2*Z*-ethylidenepiperidine –5.1/*3.6* (**8s**-S1)

[a] Total barriers and reaction energies are relative to the prevalent form of the Cp*$_2$Sm–amido catalyst complex, *viz*. Cp*$_2$Sm–amido–(substrate)] adduct **3**-S1 and the appropriate number of substrate molecules. [b] Enthalpies and free energies of activation ($\Delta H^{\ddagger}/\Delta G^{\ddagger}$) and reaction ($\Delta H/\Delta G$) are given in kilocalories per mole; numbers in italic type are the Gibbs free energies. [c] See Schemes 4, 5. [d] See the text (or Fig. S7) for description of the various isomers of the amine adduct **5'**-S2 and of the Cp*$_2$Sm–amido–cycloamine product species, respectively. [e] To engage the isomer of **5'**-S2 generated through the central ring-closure trajectory (see Scheme S2). [f] To engage the isomer of **5'**-S2 generated through the lateral ring-closure trajectory (see Scheme S2). [g] The isomer of **5'**-S2 generated through the frontal ring-closure trajectory cannot traverse this pathway.

Computational Details

All calculations have been performed with the program package TURBOMOLE[1] using Kohn-Sham density functional theory[2] (DFT). The almost nonempirical meta-GGA Tao–Perdew–Staroverov–Scuseria (TPSS)[3] was used together with the RI-*J* approximation.[4] The good to excellent performance of the TPSS functional for a wide range of applications has been demonstrated previously.[5] In view of the fact that all species investigated in this study show a large HOMO−LUMO gap, a spin-restricted formalism was used for all the calculations.

For Sm we used the Stuttgart−Dresden scalar-relativistic pseudopotential (SDD, 51 core electrons)[6] in combination with the (7s6p5d1f)/[5s4p3d1f] valence basis set contracted according to a (31111/3111/311/1) scheme.[6] This pseudopotential treats [Kr]4d^{10}4f^{5} as a fixed core, whereas 5s^{2}5p^{6}6s^{2}5d^{1}6p^{0} shells are taken into account explicitly. All remaining elements were represented by Ahlrich's valence triple-ζ TZVP basis set[7a,b] with polarization functions on all atoms.

The reaction paths were explored by the growing string method,[8] in which two string fragments (commencing from reactant and product side, respectively) are grown until the two fragments join. As this was performed in mass-weighted coordinates, an approximate to the minimum energy path (MEP) was obtained. This identified the reactant and product states to be linked to the associated transition state. The approximate saddle points connected with the MEP were subjected to an exact localisation of the TS structures. The geometry optimisation and the saddle-point search were carried out by utilising analytical/numerical gradients/Hessians according to standard algorithms. No symmetry constraints were imposed in any case. The stationary points were identified exactly by the curvature of the potential-energy surface at these points corresponding to the eigenvalues of the Hessian. All reported transition states possess exactly one negative Hessian eigenvalue, while all other stationary points exhibit exclusively positive eigenvalues. The many isomers that are possible for each of the investigated species were carefully explored. It has been explicitly scrutinized for each of the individual steps as to whether additional substrate molecules, which are present in excess, are likely serving to facilitate the elementary process.

The reaction and activation enthalpies and free energies (ΔH, $\Delta H^{\ddagger}$ and ΔG, $\Delta G^{\ddagger}$ at 298 K and 1 atm) were evaluated according to standard textbook procedures[9] using computed harmonic frequencies. The frequency analysis was performed for stationary points that were located with an alternative basis set, consisting of the aforementioned basis for La and Ahlrichs' split valence SV(P) basis set[7c] with polarisation functions on main group atoms, but not on hydrogen. This level of basis-set quality has been identified as a reliable tool for the assessment of structural parameters and vibrational frequencies,[10] thus this strategy allows an affordable and accurate determination of thermodynamic state functions. Enthalpies were reported as ΔE + zero point energy corrections at 0 K + thermal motion corrections at 298 K and Gibbs free-energies were obtained as $\Delta G = \Delta H - T\Delta S$ at 298 K.

The influence of nonspecific solute−solvent interactions[11] on both geometries and reaction energetics has been estimated for benzene (dielectric constant ε = 2.247 at 298 K)[12] by

employing the conductor-like screening model (COSMO) due to Klamt and Schüürmann[13] as implemented in TURBOMOLE.[14] The solvent excluding surface was used along with ε = 2.247 and nonelectrostatic contributions to solvation were not considered. The solvation effects were included selfconsistently in the calculations, and all key stationary species were fully optimised in the presence of the bulk solvent. The optimised atomic COSMO radii (r_H = 1.3 Å, r_C = 2.0 Å, r_N = 1.83 Å)[15] have been used, in combination with the van der Waals radius[16] (multiplied by a standard scaling factor of 1.17) for silicon; i.e. r_{Si} = 2.46 Å, and a radius of 2.22 Å for Sm. Although the Born energy reported by the COSMO model is, in a strict sense, a free energy, the entropy contributions accounts to only a very small fraction (~2%) of the total energy.[17] The solvation enthalpy was approximated by the difference between the electronic energy computed using the COSMO solvation model and the gas-phase energy. As an alternative, $H_{solution}(T)$ can be obtained from the same functional form as for $H_{gas}(T)$, but with the inertia moments and vibrational frequencies modified by solvation.[18] This gave almost identical results with an enthalpy disparity of typically less than 1 kcal mol^{-1}, but at drastically increased computational costs. The entropy contributions for condensed-phase conditions were estimated based on the computed gas-phase entropies by employing the procedure of Wertz.[19] According to this three step procedure, the solute in gas phase is first compressed to the molar volume of the solvent. The associated change in solute entropy is given by $\Delta S = R \ln(V_{m,f}/V_{m,i})$, where $V_{m,i}$ and $V_{m,f}$ are the solute molar volumes at initial and final stage; thus $\Delta S_1 = R \ln(V_{m,lig}/V_{m,gas})$ for the first step. The compressed solute then loses the same fraction of its entropy, which would be lost upon transfer from gas to liquid when the two phases have the same density, namely that of the liquid. The entropy fraction α lost here is given by $\alpha = (S_{liq}^\circ - S_{gas,ligdens})/S_{gas,ligdens}$, where the entropy of gaseous solvent at the same density as the liquid $S_{gas,ligdens}$ can be obtained from $S_{gas}^\circ + R \ln(V_{m,lig}/V_{m,gas})$. In a third step, the solute gas is expanded from the molar volume of the liquid solvent to the density of a standard solution of 1.0 L mol^{-1}, with $\Delta S_3 = R \ln(V_{m,1M}/V_{m,lig})$. Taking the experimental data for benzene,[12] the entropy fraction lost in the second step amounts to $\alpha = -0.22$.[20] On assumption that all solute molecules lose the same fraction of their entropy when transferred from gas to liquid, some simple algebraic transformation leads to the solvation entropy as given by the sum of the entropy changes associated with each of the three steps, *viz*. $\Delta S_{solv} = \Delta S_1 + \alpha(S_{gas}^\circ + \Delta S_1) + \Delta S_3$. Thus, for benzene solvent at 298 K one obtains $\Delta S_{solv} = -0.22 S_{gas}^\circ - 3.92$ cal/K•mol. Accordingly, the procedure proposed by Wertz gives rise to the following estimate for the total solute entropy (again for benzene solvent at 298 K) as expressed in terms of the gas-phase entropy:

$$S_{sol} = 0.78\ S_{gas}^\circ - 3.92 \text{ cal/K•mol} \qquad (1)$$

Although somehow empirical, the Wertz procedure provides a reasonable estimate of the entropy of a molecule in condensed phase, which is known to be less than its entropy in gaseous phase,[19–21] which may be used in a somewhat pragmatic way in the absence of reliable alternatives that are affordable. Noteworthy, this procedure has been successfully applied in several cases.[22] The strict treatment of the free-energy in condensed phase, for instance by applying non-empirical MD simulation techniques, is currently too expensive to be

carried out for a mechanistic scenario as diverse as explored herein and taking the size of the employed catalyst model also into account; this is likely to remain so in the foreseeable future.

---

1 (a) R. Ahlrichs, M. Bär, M. Häser, H. Horn, C. Kölmel, *Chem. Phys. Lett*., **1989**, **162**, 165; (b) O, Treutler, R. Ahlrichs, *J. Chem. Phys*., 1995, **102**, 346; (c) R. Ahlrichs, F. Furche, C. Hättig, W. Klopper, M. Sierka, F. Weigend, *TURBOMOLE, version 5.9*; University of Karlsruhe: Karlsruhe, Germany, 2006; http://www.turbomole.com.

2 R. G. Parr, W. Yang, W. *Density-Functional Theory of Atoms and Molecules*, Oxford University Press, 1989.

3 (a) P. A. M. Dirac, *Proc. Royal Soc. (London)*, 1929, **A123**, 714; (b) J. C. Slater, *Phys. Rev*., 1951, **81**, 385; (c) J. P. Perdew. Y. Wang, *Phys. Rev*., 1992, **B45**, 13244; (d) J. Tao, J. P. Perdew, V. N. Staroverov, G. E. Scuseria, *Phys. Rev. Lett*., 2003, **91**, 146401; (e) J. P. Perdew, J. Tao, V. N. Staroverov, G. E. Scuseria, *J. Chem. Phys*., 2004, **120**, 6898.

4 (a) O. Vahtras, J. Almlöf, M. W. Feyereisen, *Chem. Phys. Lett*., 1993, **213**, 514; (b) K. Eichkorn, O. Treutler, H. Öhm, M. Häser, R. Ahlrichs, *Chem. Phys. Lett*., 1995, **242**, 652.

5 (a) V. N. Staroverov, G. E. Scuseria, J. Tao, J. P. Perdew, *J. Chem. Phys*., 2003, **119**, 12129; (b) Y. Zao, D. G. Truhlar, *J. Chem. Theory Comput*., 2005, **1**, 415; (c) F. Furche, J. P. Perdew, *J. Chem. Phys*., 2006, **124**, 044103.

6 M. Dolg, H. Stoll, A. Savin, H. Preuß, *Theor. Chim. Acta*, 1989, **75**, 173.

7 (a) A. Schäfer, C. Huber, R. Ahlrichs, *J. Chem. Phys*., 1994, **100**, 5829; (b) K. Eichkorn, F. Weigend, O. Treutler, R. Ahlrichs, *Theor*. *Chem*. *Acc*., 1997, **97**, 119; (c) A. Schäfer, C. Huber, R. Ahlrichs, *J. Chem. Phys*., 1992, **97**, 2571.

8 (a) B. Peters, A. Heyden, A. T. Bell, A. Chakraborty, *J. Chem. Phys*., 2004, **120**, 7877; (b) A. Heyden, *personal communication*.

9 D. A. McQuarrie, *Statistical Thermodynamics*, Harper & Row, New York, 1973.

10 W. Koch, M. C. Holthausen, *A Chemist's Guide to Density Functional Theory*, 2nd Ed., Wiley-VCH, Weinheim, 2001.

11 (a) J. Tomasi, M. Persico, *Chem. Rev*., 1994, **94**, 2027; (b) C. J. Cramer, D. G. Truhlar, *Chem. Rev*., 1999, **99**, 2161; (c) C. J. Cramer, *Essentials of Computational Chemistry: Theories and Models*; John Wiley & Sons : Chincester, U.K., 2002, pp 347–383.

12 *CRC Handbook of Chemistry and Physics* (Ed.: D. R. Lide), 84th ed. CRC Press, New York, 2003–2004.

13 (a) A. Klamt, G. Schüürmann, *J. Chem. Soc. Perkin Trans. 2*, 1993, 799; (b) A. Klamt, in *Encyclopaedia of Computational Chemistry* (Ed,: P. v. R. Schleyer), John Wiley, & Sons: Chichester, 1998; Vol. 1, pp. 604 –615.

14 A. Schäfer, A. Klamt, D. Sattel, J. C. W. Lohrenz, F. Eckert, *Phys. Chem. Chem. Phys*., 2000, **2**, 2187.

15 A. Klamt, V. Jonas, Th. Bürger, J. C. W. Lohrenz, *J. Phys. Chem. A*, 1998, **102**, 5074.

16 A. Bondi, *J. Phys. Chem.*, 1964, **68**, 441.

17 W. E. Dasent, *Inorganic Energetics*, Penguin, Middlesex, UK, 1970.

18 A. Klamt, *J. Phys. Chem*., 1996, **100**, 3349.

19 D. H. Wertz, *J. Am. Chem. Soc*., 1980, **102**, 5316.

20 M. H. Abraham, *J. Am. Chem. Soc*., 1981, **103**, 6742.

21 (a) V. Cabani, P. Gianni, V. Mollica, L. Lepori, *J. Solution Chem*., 1981, **10**, 563; (b) D. D. Wagman, W. H. Evans, V. B. Parker, R. H. Schumm, I. Halow, S. M. Bailey, K. L. Churney, R. L. Nuttall, *J. Phys. Ref. Data*, 1982, **11**, Supplement No. 2; (c) A. Ben-Naim, Y. Marcus, *J. Chem. Phys*., 1984, **81**, 2016; (d) Y. Okuno, *Chem. Eur. J*., 1997, **3**, 212; (e) W. R. Fawcett, *J. Phys. Chem. B*, 1999, **103**, 11181.

22 (a) I. H. Williams, D. Spangler, D. A. Femec, G. M. Maggiora, R. L. Schowen, *J. Am. Chem. Soc*., 1983, **105**, 31; (b) I. H. Williams, *J. Am. Chem. Soc*., 1987, 109, 6299; (c) S. Wolfe, Ch-K. Kim, K. Yang, N. Weinberg, Z. Shi, *J. Am. Chem. Soc*., 1995, **117**, 4240; (d) J. Cooper, T. Ziegler, *Inorg. Chem*., 2002, **41**, 6614; (e) I. H. Hristov, T. Ziegler, *Organometallics*, 2003, **22**, 3515; (f) J. K.-C. Lau, D. V. Deubel, *Chem. Eur. J*., 2005, **11**, 2849; (g) S.-T.Lin, P. K. Maiti, W. A. Goddard, III, *J. Phys. Chem. B*, 2005, **109**, 8663; (f) H. Zhu, T. Ziegler, *J. Organomet. Chem*., 2006, **691**, 4486; (h) J. K.-C. Lau, D. V. Deubel, *J. Chem. Theory Comp*., 2006, **2**, 103; (i) D. V. Deubel, *J. Am. Chem. Soc*., 2006, **128**, 1654.

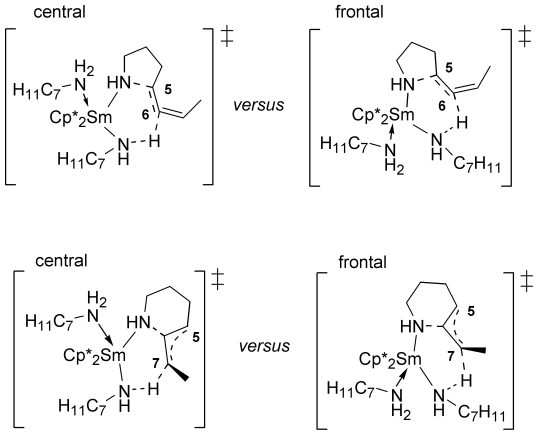

Scheme S1 Alternative trajectories for *exo*- (top) and *endo*cyclic (bottom) non-insertive C–N ring closure with concomitant amino proton delivery onto the allene unit in **3**-S2.

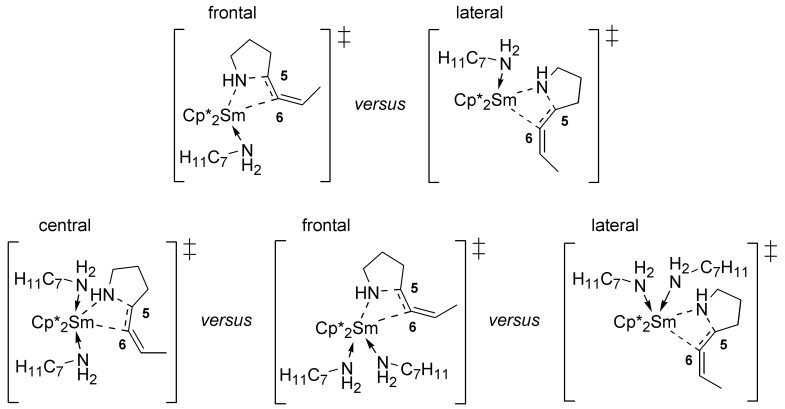

Scheme S2 Alternative trajectories for *exo*cyclic ring closure through migratory allene insertion into the Sm–N amido σ-bond in **3**-S1 (top) and **3**-S2 (below).

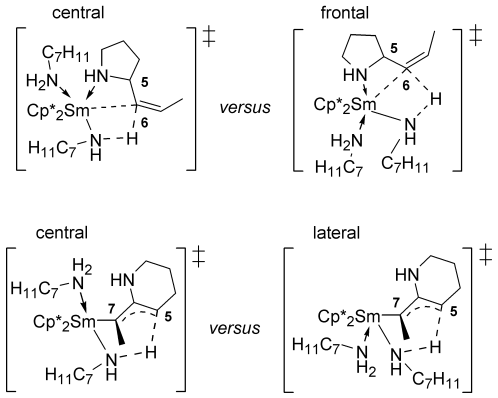

Scheme S3 Alternative trajectories for Sm–C^6 bond aminolysis commencing from **4**-S2 (top) and Sm–C^5 bond aminolysis commencing from **5'**-S2 (bottom).

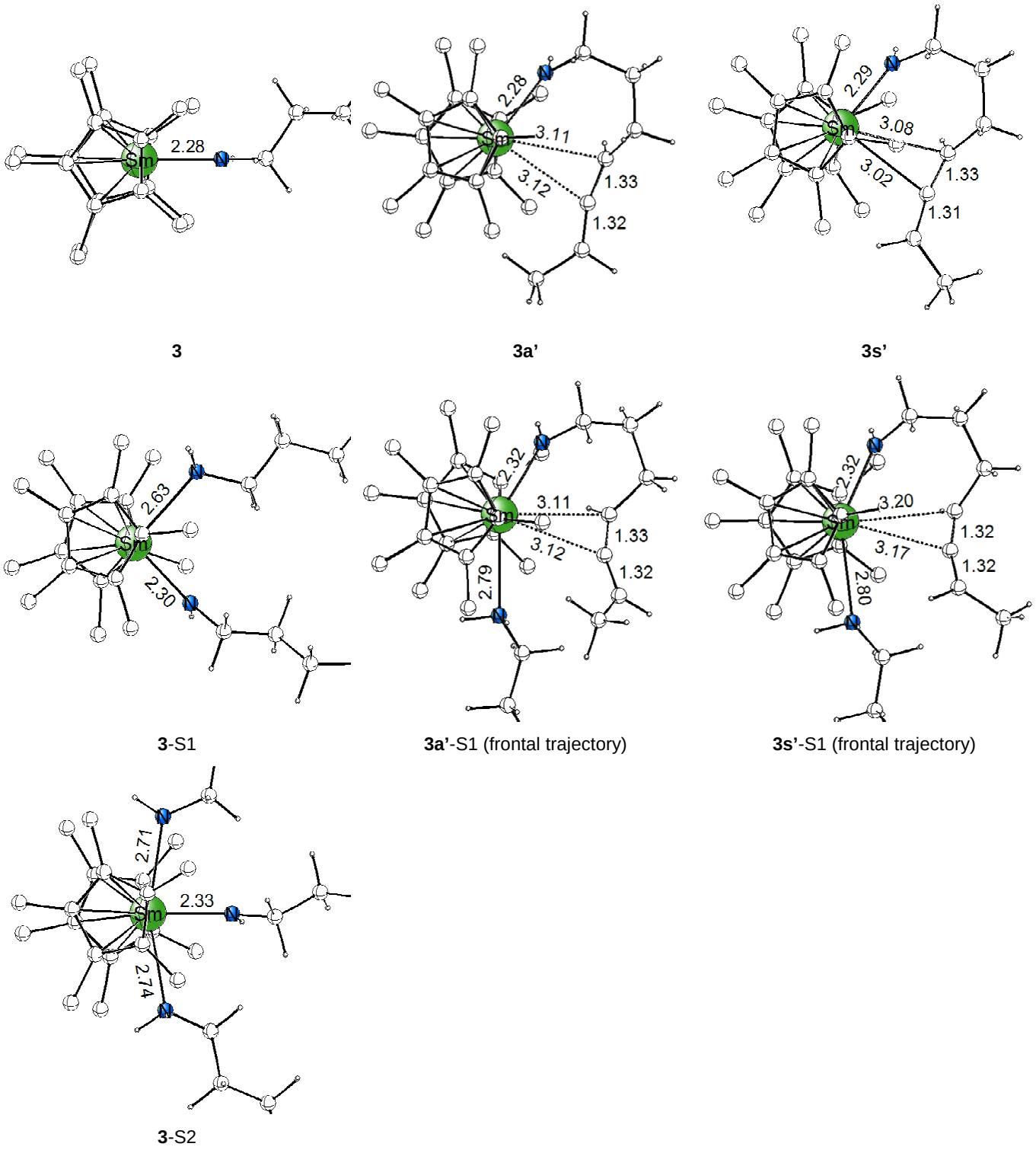

Fig. S1 Selected structural parameter (Å) of the optimised structures of various forms of the catalytically competent Cp^*_2Sm–amidoallene complex. See Tables S2a–S2c for the energetics. The cut-off for drawing Sm–C bonds was arbitrarily set to 3.1 Å. The hydrogen atoms on the methyl groups of the Cp^*_2Sm backbone are omitted for the sake of clarity. Note that some of the amino/amidoallene units are displayed in a truncated fashion for several of the species.

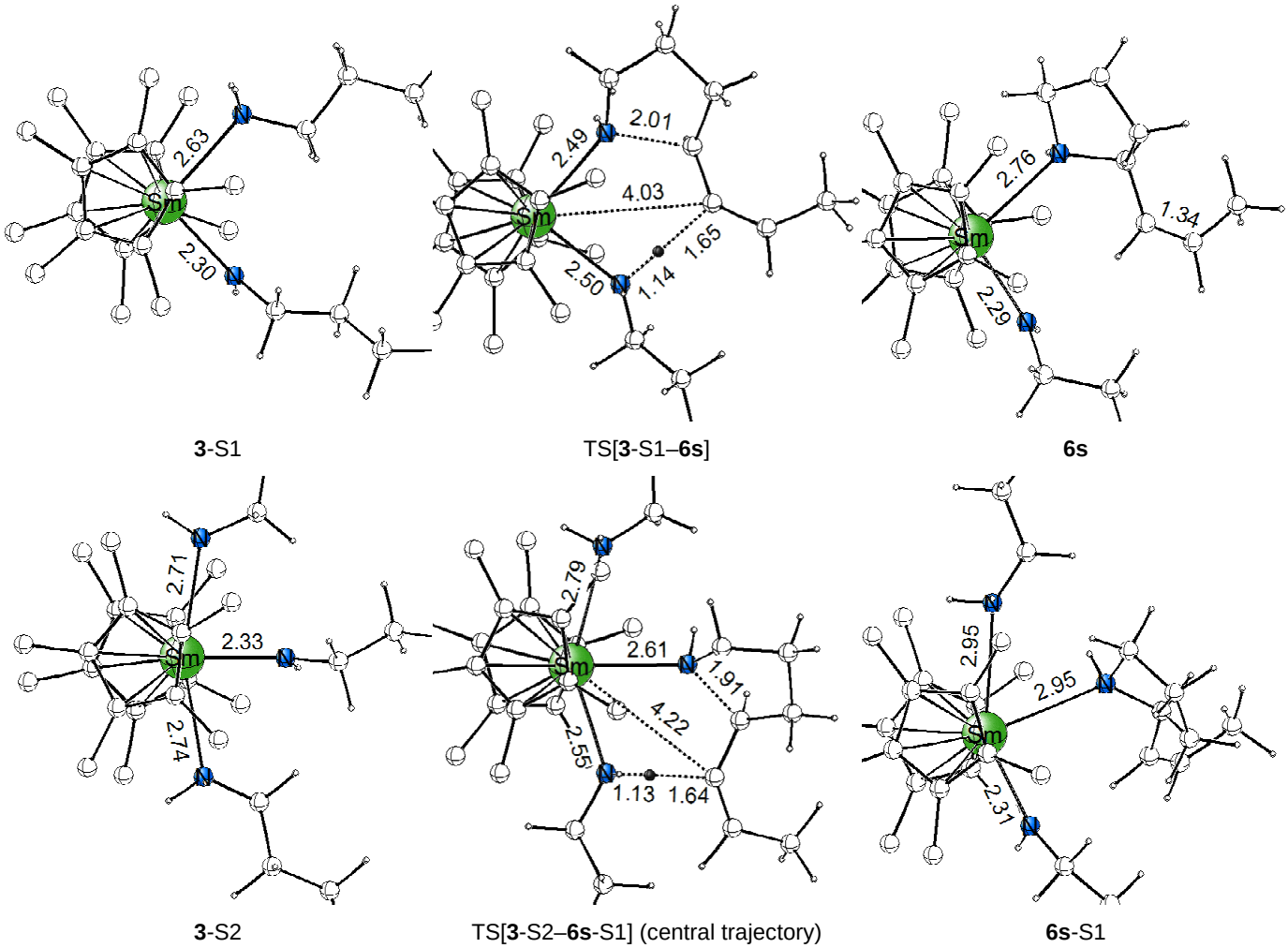

3-S1 TS[**3**-S1–**6s**] **6s**

3-S2 TS[**3**-S2–**6s**-S1] (central trajectory) **6s**-S1

Fig. S2 Selected structural parameter (Å) of the optimised structures of key stationary points for non-insertive *exo*cyclic C^5–N ring closure with concurrent amino proton delivery onto the allene-C^6 centre in **3**-S1 (*syn* pathway, top) and in **3**-S2 (*syn* pathway, bottom). See Tables S1a, S1b for the energetics. The cut-off for drawing Sm–C bonds was arbitrarily set to 3.1 Å. The hydrogen atoms on the methyl groups of the Cp^*_2Sm backbone are omitted for the sake of clarity. Note that some of the amino/amidoallene units are displayed in a truncated fashion for several of the species.

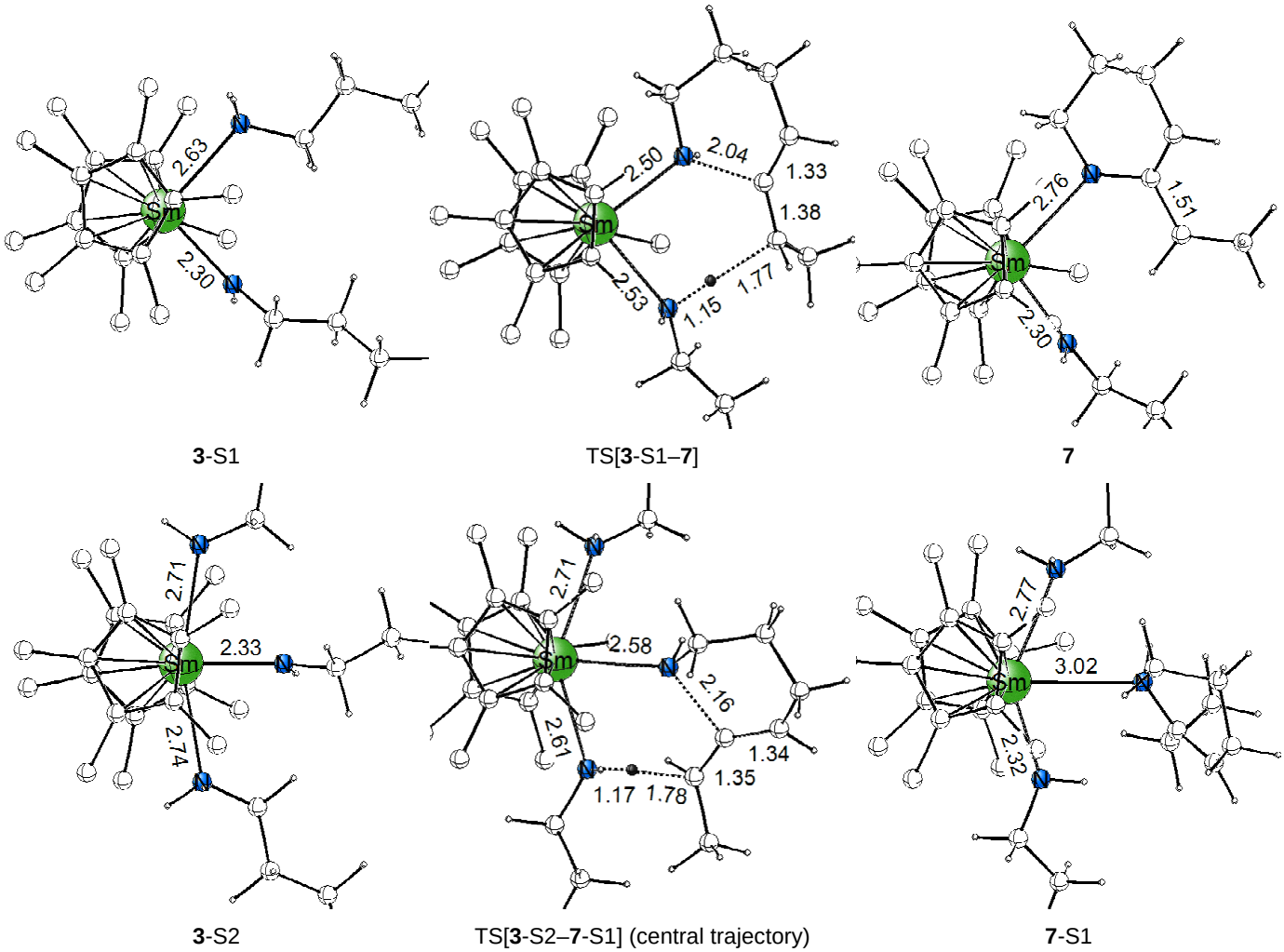

3-S1 TS[**3**-S1–**7**] **7**

3-S2 TS[**3**-S2–**7**-S1] (central trajectory) **7**-S1

Fig. S3 Selected structural parameter (Å) of the optimised structures of key stationary points for non-insertive *endo*cyclic C^6–N ring closure with concurrent amino proton delivery onto the allene-C^7 centre in **3**-S1 (*syn* pathway, top) and in **3**-S2 (*anti* pathway, bottom). See Tables S1a, S1b for the energetics. The cut-off for drawing Sm–C bonds was arbitrarily set to 3.1 Å. The hydrogen atoms on the methyl groups of the Cp^*_2Sm backbone are omitted for the sake of clarity. Note that some of the amino/amidoallene units are displayed in a truncated fashion for several of the species.

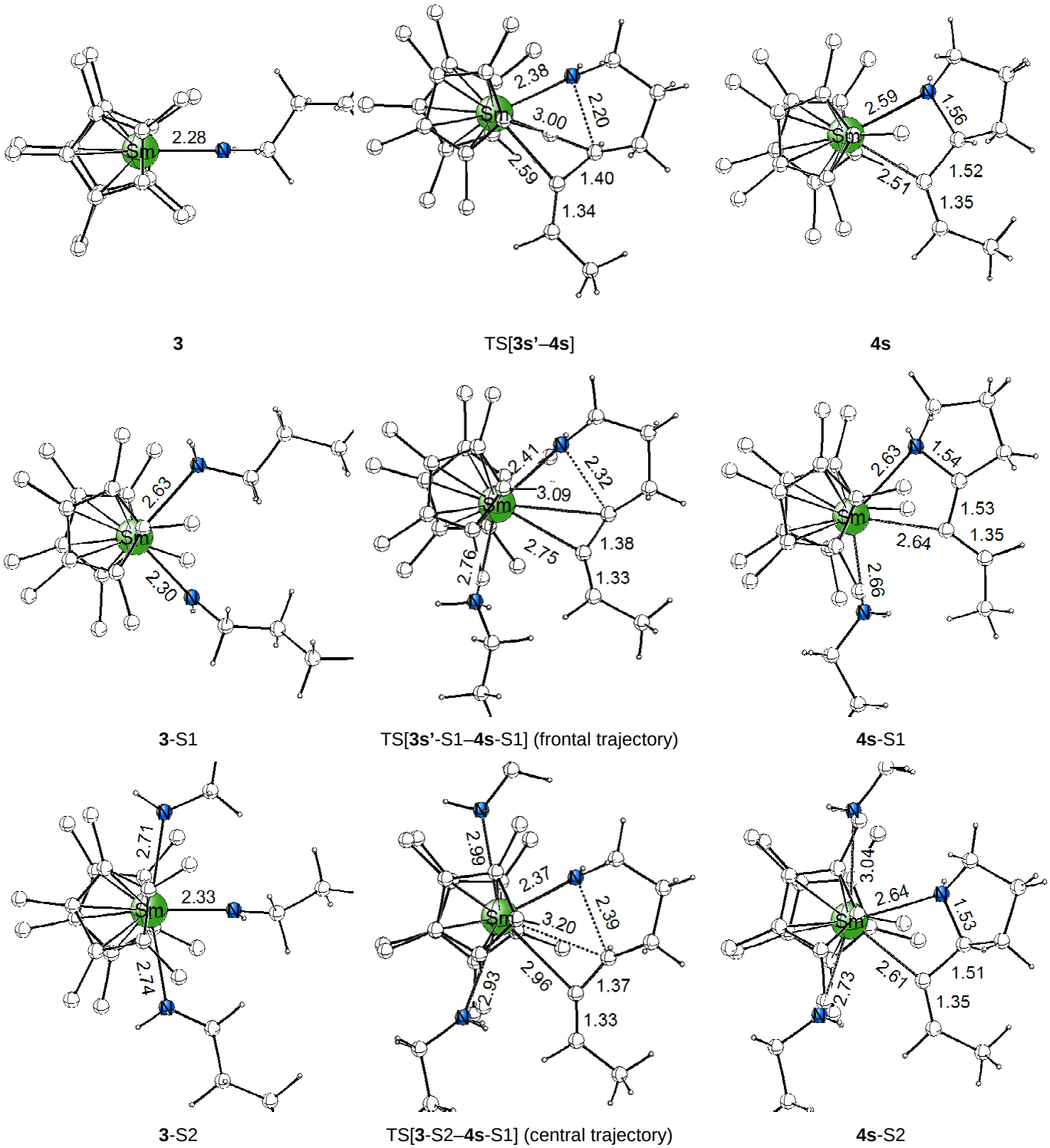

3 TS[**3s'**–**4s**] **4s**

3-S1 TS[**3s'**-S1–**4s**-S1] (frontal trajectory) **4s**-S1

3-S2 TS[**3**-S2–**4s**-S1] (central trajectory) **4s**-S2

Fig. S4 Selected structural parameter (Å) of the optimised structures of key stationary points for *exo*cyclic C^5–N ring closure through migratory allene insertion into the Sm–N amido σ-bond in substrate-free **3** (*syn* pathway, top), in **3**-S1 (*syn* pathway, middle) and in **3**-S2 (*syn* pathway, bottom). See Tables S2a–S2c for the energetics. The cut-off for drawing Sm–C bonds was arbitrarily set to 3.1 Å. The hydrogen atoms on the methyl groups of the Cp^*_2Sm backbone are omitted for the sake of clarity. Note that some of the amino/amidoallene units are displayed in a truncated fashion for several of the species.

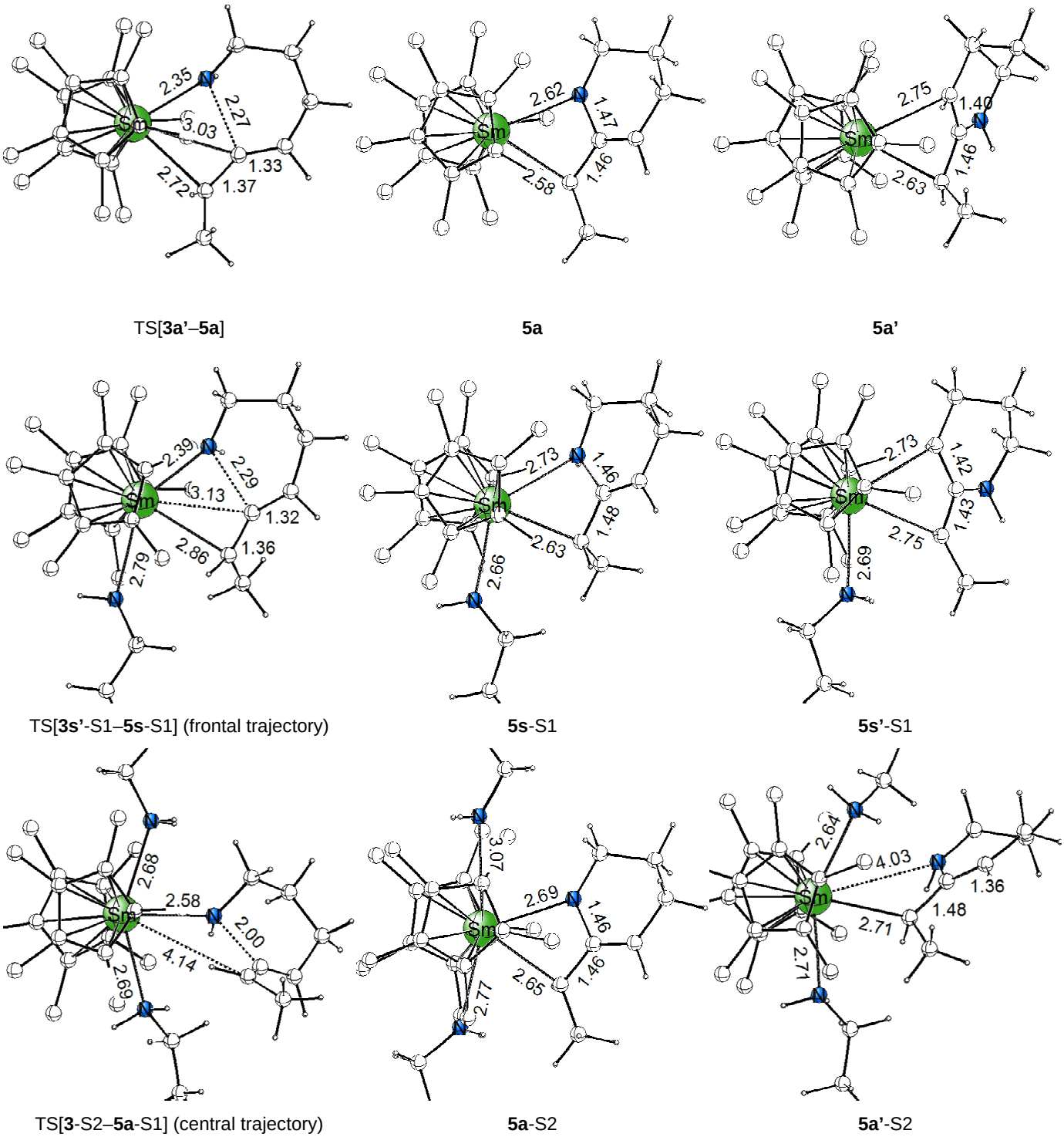

TS[**3a'**–**5a**] **5a** **5a'**

TS[**3s'**-S1–**5s**-S1] (frontal trajectory) **5s**-S1 **5s'**-S1

TS[**3**-S2–**5a**-S1] (central trajectory) **5a**-S2 **5a'**-S2

Fig. S5 Selected structural parameter (Å) of the optimised structures of key stationary points for *endo*cyclic C^6–N ring closure through migratory allene insertion into the Sm–N amido σ-bond in substrate-free **3** (*anti* pathway, top), in **3**-S1 (*syn* pathway, middle) and in **3**-S2 (*anti* pathway, bottom). See Tables S2a–S2c for the energetics. The cut-off for drawing Sm–C bonds was arbitrarily set to 3.1 Å. The hydrogen atoms on the methyl groups of the Cp^*_2Sm backbone are omitted for the sake of clarity. Note that some of the amino/amidoallene units are displayed in a truncated fashion for several of the species.

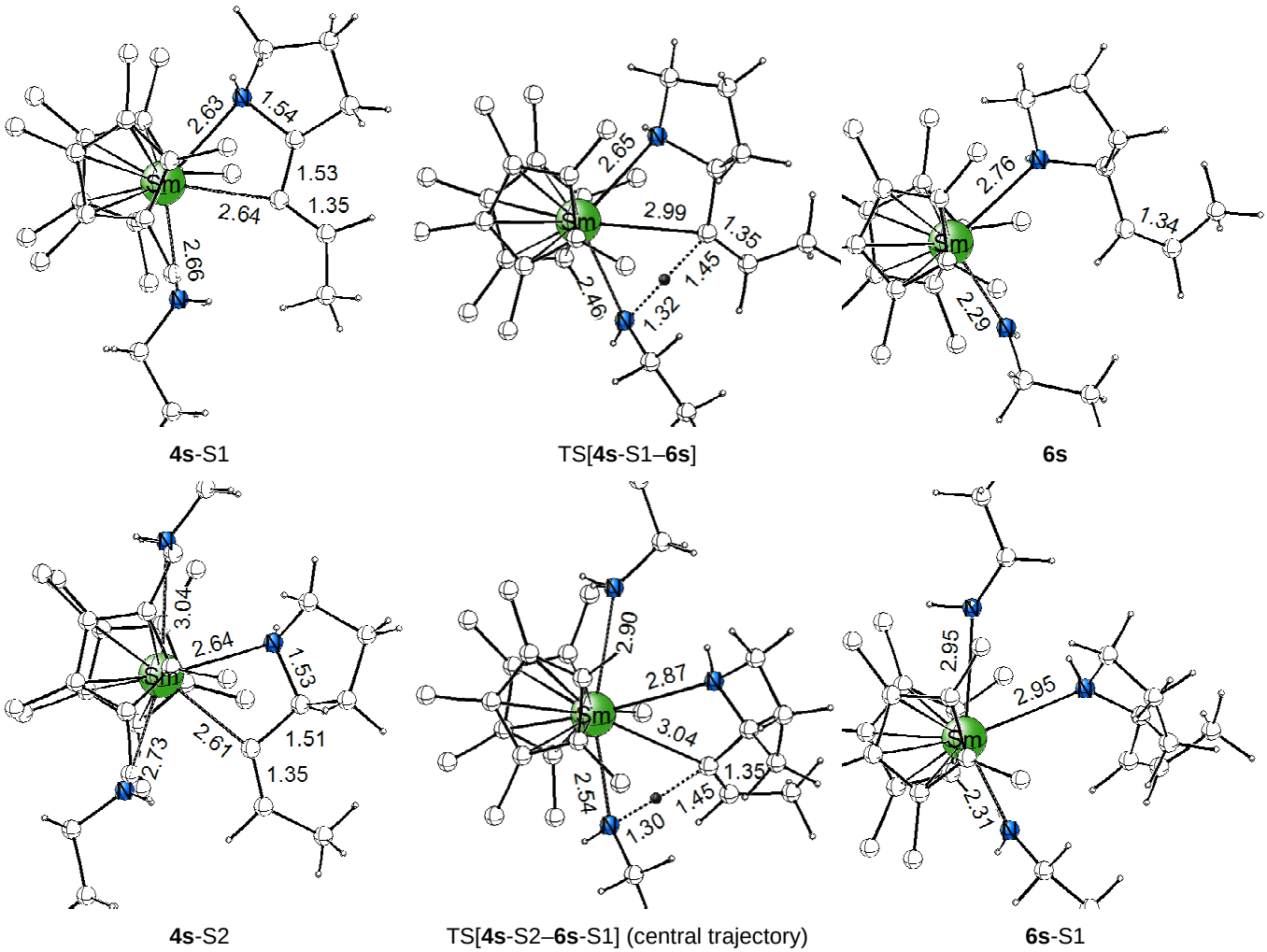

Fig. S6 Selected structural parameter (Å) of the optimised structures of key stationary points for protonation of the azacycle's tether in **4s**-S1 (top) and in **4s**-S2 (bottom) through the most accessible trajectories. See Tables S4a, S4b for the energetics. The cut-off for drawing Sm–C bonds was arbitrarily set to 3.1 Å. The hydrogen atoms on the methyl groups of the Cp^*_2Sm backbone are omitted for the sake of clarity. Note that some of the amino/amidoallene units are displayed in a truncated fashion for several of the species.

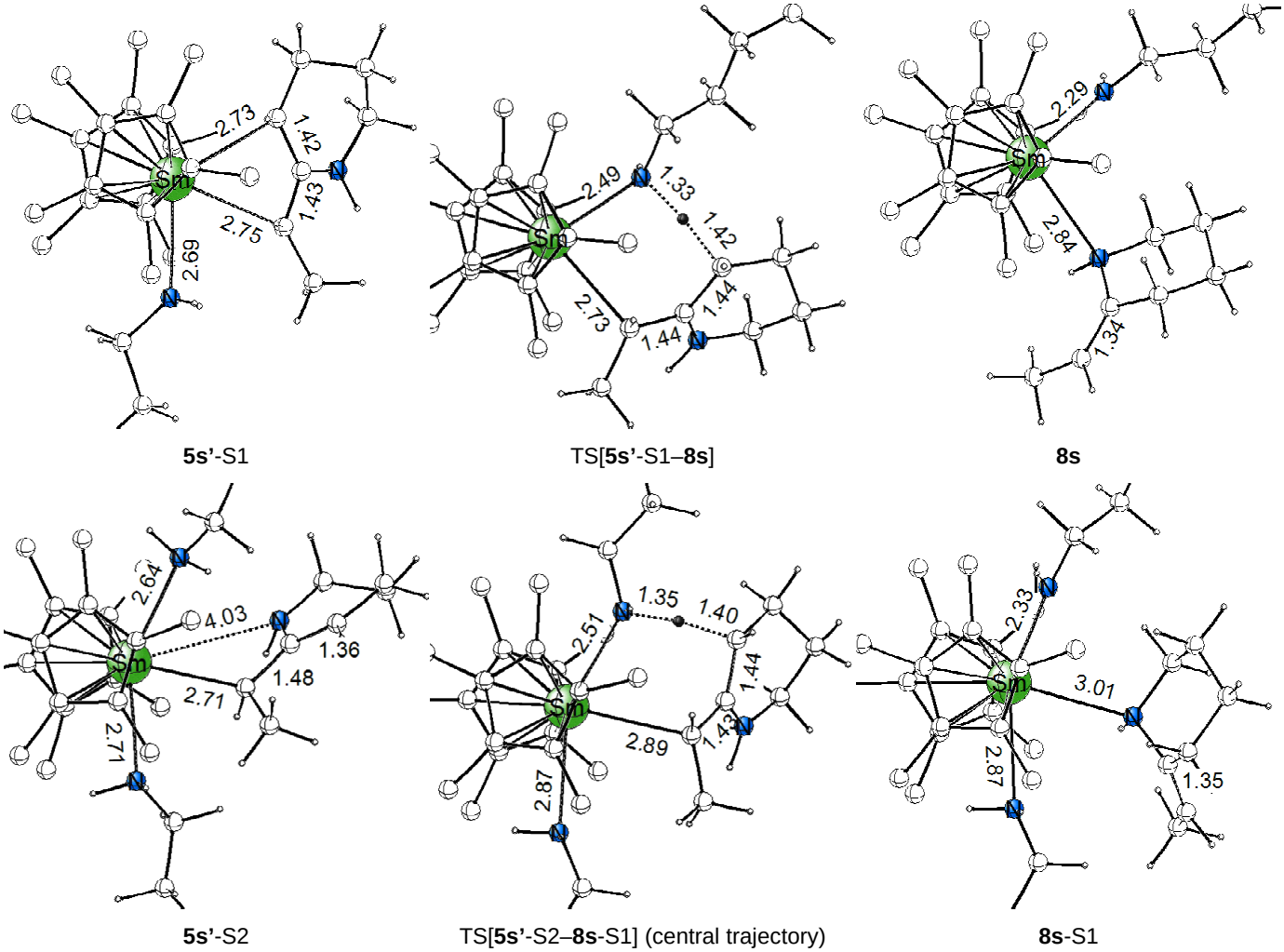

5s'-S1 TS[**5s'**-S1–**8s**] **8s**

5s'-S2 TS[**5s'**-S2–**8s**-S1] (central trajectory) **8s**-S1

Fig. S7 Selected structural parameter (Å) of the optimised structures of key stationary points for protonation of the azacycle's tether in **5s'**-S1 (top) and in **5s'**-S2 (bottom) through the most accessible trajectories. See Tables S4a, S4b for the energetics. The cut-off for drawing Sm–C bonds was arbitrarily set to 3.1 Å. The hydrogen atoms on the methyl groups of the Cp^*_2Sm backbone are omitted for the sake of clarity. Note that some of the amino/amidoallene units are displayed in a truncated fashion for several of the species.